

Hybrid Beamforming Design for RSMA-enabled Near-Field Integrated Sensing and Communications

Jiasi Zhou, Cong Zhou, Chintha Tellambura, *Fellow, IEEE*, and Geoffrey Ye Li, *Fellow, IEEE*

Abstract—To enable high data rates and sensing resolutions, integrated sensing and communication (ISAC) networks leverage extremely large antenna arrays and high frequencies, extending the Rayleigh distance and making near-field (NF) spherical wave propagation dominant. This unlocks numerous spatial degrees of freedom, raising the challenge of optimizing them for communication and sensing tradeoffs. To this end, we propose a rate-splitting multiple access (RSMA)-based NF-ISAC transmit scheme utilizing hybrid digital-analog antennas. RSMA enhances interference management, while a variable number of dedicated sensing beams adds beamforming flexibility. The objective is to maximize the minimum communication rate while ensuring multi-target sensing performance by jointly optimizing receive filters, analog and digital beamformers, common rate allocation, and the sensing beam count. To address uncertainty in sensing beam allocation, a rank-zero solution reconstruction method demonstrates that dedicated sensing beams are unnecessary for NF multi-target detection. A penalty dual decomposition (PDD)-based double-loop algorithm is introduced, employing weighted minimum mean-squared error (WMMSE) and quadratic transforms to reformulate communication and sensing rates. Simulations reveal that the proposed scheme: 1) Achieves performance comparable to fully digital beamforming with fewer RF chains, 2) Maintains NF multi-target detection without compromising communication rates, and 3) Significantly outperforms space division multiple access (SDMA) and far-field ISAC systems.

Index Terms—Near-field communications, integrated sensing and communication, rate splitting multiple access.

I. INTRODUCTION

Future wireless networks aim to deliver immense throughput and high-accuracy sensing to support autonomous driving, smart healthcare, and other emerging applications [1]. The integrated sensing and communication (ISAC) paradigm facilitates the dual use of radio signals and wireless infrastructure [1], [2]. To meet these demands, ISAC is advancing towards extremely large-scale antenna arrays (ELAA) and high-frequency bands to enhance communication capacity and sensing resolution [3].

Jiasi Zhou is with the School of Medical Information and Engineering, Xuzhou Medical University, Xuzhou, 221004, China, (email: jiasi_zhou@xzhmu.edu.cn). (*Corresponding author: Jiasi Zhou*).

Cong Zhou is with the School of Electronic and Information Engineering, Harbin Institute of Technology, Harbin 150001, China, (email: zhoucong@stu.hit.edu.cn).

Chintha Tellambura is with the Department of Electrical and Computer Engineering, University of Alberta, Edmonton, AB, T6G 2R3, Canada (email: ct4@ualberta.ca).

Geoffrey Ye Li is with the School of Electrical and Electronic Engineering, Imperial College London, London SW7 2AZ, UK (e-mail: geoffrey.li@imperial.ac.uk).

This work was supported by the national key research and development program of China (2020YFC2006600) and the Talented Scientific Research Foundation of Xuzhou Medical University (D2022027).

These advancements fundamentally alter electromagnetic (EM) characteristics [4]. Specifically, the EM radiation region around transmit antennas is divided into far-field (FF) and near-field (NF) zones, separated by the Rayleigh distance. FF channels exhibit plane-wave propagation, while NF channels are characterized by spherical-wave propagation [5]. With ELAA and high-frequency operation, the Rayleigh distance can extend to several tens or hundreds of meters, making spherical-wave propagation dominant. Unlike plane-wave propagation, spherical waves introduce an additional distance dimension, incorporating both direction and distance information [5]. This enables NF beamforming to focus energy on specific points, significantly boosting throughput and connectivity. This shift opens new possibilities for ISAC systems but highlights limitations of existing FF-ISAC studies [1], [2], [6], [7], which may not align with real-world wireless propagation properties. Rethinking and redesigning ISAC systems is therefore essential to exploiting these capabilities fully.

The coexistence of communication and sensing networks in ISAC creates a complex wireless environment, making effective interference management critical [8]. Common approaches include space division multiple access (SDMA) and non-orthogonal multiple access (NOMA). SDMA treats interference as noise, while NOMA decodes all stronger interference signals. However, both lack flexibility and fail to deliver precise interference management, limiting network performance [9]–[11]. Rate-splitting multiple access (RSMA) offers a more robust and adaptable solution by allowing receivers to partially decode interference while tolerating residual interference. This approach achieves higher spectral efficiency and fairness compared to SDMA and NOMA [12], [13]. Additionally, by adjusting the interference decoding percentage, RSMA generalizes SDMA and NOMA as special cases [9], [14]. Integrating RSMA with NF-ISAC holds significant potential for performance gains and warrants further investigation.

A. Related works

Many studies mainly consider FF-ISAC designs, where the sensing performance is evaluated by Cramér-Rao bound (CRB) [1], [2], [15], detection rate [7], [16], [17], or transmit beam pattern [18]. Specifically, The authors in [1] study the complete response matrix and reflection angle estimations corresponding to target detection and tracking stages. These two sensing models are extended to simultaneous wireless information and power transfer (SWIPT)-enabled ISAC networks in [2]. Imperfect channel state information (SCI) and on-off control of non-transmission power are respectively considered

in [7] and [15] to enhance robustness and energy efficiency. Besides, ISAC can integrate with other technologies. For example, multiple base stations (BS) can be cooperatively scheduled in cell-free networks to provide multi-angle observations and higher spatial diversity [16]. Intelligent omni-surfaces (IOS) can achieve seamless 360-degree coverage in multi-target detection [17]. These contributions exploit spatial multiplexing gains to counter interference. However, when many users are scheduled per time slot, excess interference saturates the network performance [19]. To elevate performance, the authors in [20], [21] design NOMA-aided ISACs. However, the limited gains require stringent decoding order, complex receiver designs, and large channel gain differences.

RSMA can overcome rate saturation and reduce receiver complexity. It achieves higher energy efficiency [22], higher fairness rate [23], better robustness [24], and higher sum rate [25] over SDMA and NOMA. Given these benefits, RSMA has been exploited for ISAC networks in [8], [26]–[30]. For example, RSMA is investigated to detect multiple moving targets for mono-static ISAC systems, where a general CRB sensing metric is derived [27]. To enhance beampattern matching capacity, reference [26] injects an additional radar sequence and utilizes RSMA to control the interference level between the radar sequence and communication streams. Apart from injecting radar sequences, the common stream of RSMA can be independently designed to enhance sensing performance [8]. In addition, RSMA-enabled ISAC can be extended to reconfigurable intelligence surface (RIS) [29], cloud radio access networks (C-RAN) [28], and satellite systems [30]. However, these efforts mainly focus on **the FF regime**.

The NF-ISAC remains largely unexplored, except for [31]–[35]. Communication and dedicated sensing beamforming in single-target scenarios are jointly designed to optimize the beampattern [36]. A multi-target detection approach is developed in [32], where the sensing rate is used as the evaluation metric. However, these two works utilize fully digital antennas, requiring high radio frequency (RF) chain costs. To attack this issue, the authors in [33] adopt a hybrid array architecture and derive the CRB for the NF joint distance and angle estimation. Furthermore, the authors in [34] propose a double-array structure for downlink and uplink ISAC, where a small-scale assisting transceiver is attached to the large-scale main transceiver to empower ISAC. Current NF-ISAC works employ SDMA to manage interference, which may experience performance saturation [32]–[36]. RSMA has presented considerable benefits in NF communications [37]. However, to the best of our knowledge, the great potential of RSMA in NF-ISAC has not been unlocked.

B. Motivations and Contributions

Although the synergy between NF-ISAC and RSMA may boost performance gains, several problems and challenges must be addressed.

- ISAC systems inherently face a tradeoff between communication and target detection tasks. Optimizing this tradeoff requires efficiently allocating spatial beams generated by the multi-antenna base station. A key challenge

is determining the optimal number of beams for communication versus target detection. This issue remains insufficiently explored, even in FF-ISAC systems, and is even more complex in NF-ISAC networks.

NF systems utilize spherical-wave-based beams, enabling array radiation patterns to concentrate energy on specific locations. This capability enhances communication by focusing power on user positions [5]. However, such focused beams may not be well-suited for supporting NF multi-target detection, as their energy concentration limits broader sensing coverage. Consequently, additional dedicated sensing beams may be crucial to achieve optimal sensing performance in NF-ISAC systems.

- Another significant challenge is the substantial RF chain deployment. An RF chain comprises a power amplifier, a digital filter, a digital-to-analog converter (DAC), and a mixer. DACs dominate the total power consumption and the RF chain is expensive [38]. The NF-ISAC typically occurs in high-frequency and ELAA scenarios. Moreover, the fully digital beamforming requires each antenna to be connected to a dedicated RF chain [5]. This results in substantially high design complexity, energy consumption, and cost [39], so the fully digital beamforming becomes prohibitively expensive and power-thirsty. As a result, this calls for hybrid beamforming architecture.

To tackle these challenges, this work proposes a novel NF-ISAC transmit scheme with a hybrid beamforming architecture, leveraging RSMA for flexible interference management. A key focus is determining whether dedicated sensing beams are necessary for NF multi-target detection, leading to the development of optimized hybrid beamforming algorithms. Table I compares our main contributions against existing ISAC studies. They are outlined below:

- A novel RSMA-enabled NF-ISAC system is proposed, where the BS simultaneously serves multiple communication users and detects numerous targets. To achieve this, the system employs a hybrid beamforming architecture. The primary objective is to maximize the minimum communication rate while satisfying transmit power constraints and ensuring the required sensing performance for multi-target detection. This involves the joint optimization of several critical components, including receive filters, the analog beamformer, digital communication and sensing beamformers, common rate allocation, and the allocation of dedicated sensing beams.
- An optimal solution reconstruction approach is developed to ascertain the impact of the number of dedicated sensing beams on the sensing rate. Specifically, an equivalent solution that produces the same objective value can always be constructed with the known optimal digital communication and sensing beamformers. Furthermore, the reconstructed sensing beamformer exhibits a rank-zero structure, indicating that dedicated sensing beams are unnecessary for NF multi-target detection.
- Building on the above insight, the focus shifts to optimizing analog and digital communication beamformers, receive filters, and common rate allocation. To achieve

TABLE I: Our contributions in contrast to the existing ISAC designs

	[1], [2], [7], [15]–[18], [20], [21]	[8], [26]–[30]	[32], [36]	[33]–[35]	Our work
NF effect	✗	✗	✓	✓	✓
RSMA	✗	✓	✗	✗	✓
Hybrid beamforming	✗	✗	✗	✓	✓
Uncertain sensing beam count	✗	✗	✗	✗	✓

this, auxiliary variables are introduced, and a penalty dual decomposition (PDD)-based double-loop algorithm is developed. Specifically, the weighted minimum mean-squared error (WMMSE) and quadratic transform methods are employed to recast communication and sensing rates into easily optimized constraints. Then, the introduced auxiliary variable is solved via a convex optimization framework. Additionally, the optimal analog beamformer, digital beamformer, and receive filters are derived with closed-form expressions.

- Extensive simulations highlight three key advantages of the proposed scheme over four competing benchmarks:
 - 1) **Efficiency in Hardware Utilization:** performance comparable to a fully digital beamformer is achieved while significantly reducing the required RF chains.
 - 2) **Balanced Dual Functionality:** effective multi-target detection in NF-ISAC systems is demonstrated without degrading communication performance.
 - 3) **Superior Performance Gains:** The scheme outperforms both SDMA and FF-ISAC approaches, demonstrating substantial improvements in overall system efficiency and capability.

Organization: The remainder of this paper is organized as follows. Section II elaborates on the system model and formulates the optimization problem. Section III rigorously proves that dedicated sensing beams are not required for NF multi-target detection. Section IV presents the proposed iterative optimization algorithm and analyzes its properties. Section IV provides simulation results. Section V concludes this paper.

Notations: Boldface upper-case letters, boldface lower-case letters, and calligraphy letters denote matrices, vectors, and sets, respectively. The $N \times K$ dimensional complex matrix space is denoted by $\mathbb{C}^{N \times K}$. Superscripts $(\bullet)^T$ and $(\bullet)^H$ represent the transpose and Hermitian transpose, respectively. $\text{Re}(\bullet)$, $\text{Tr}(\bullet)$, $\text{rank}(\bullet)$, and $\mathbb{E}[\bullet]$ denote the real part, trace, rank, and statistical expectation, respectively. Operator $\lfloor a \rfloor$ is the largest integer not greater than a . $\mathcal{CN}(\mu, \sigma^2)$ denotes a complex Gaussian of mean μ and variance σ^2 .

II. SYSTEM MODEL AND PROBLEM FORMULATION

As per Fig. 1, an RSMA-assisted NF-ISAC network comprises a dual-functional base station (BS), K single-antenna communication users, and M sensing targets. The sets of communication users and sensing targets are indexed by $\mathcal{K} = \{1, \dots, K\}$ and $\mathcal{M} = \{1, \dots, M\}$, respectively. The

BS is equipped with a uniform linear array (ULA) of N_t -transmit and N_r -receive antennas with an antenna spacing of d . The boundary between NF and FF regions is determined by Rayleigh distance $d_i = \frac{2D_i^2}{\lambda}$ for $\forall i \in \{t, r\}$, where $D_i = (N_i - 1)d$ and λ are antenna aperture and signal wavelength, respectively. All users and targets are assumed to be located in the NF region. In NF-ISAC, fully digital beamforming is impractical since allocating a dedicated RF chain to each antenna is difficult. This paper adopts the hybrid beamforming architecture to attack this issue, as shown in the left half of Fig. 1. Specifically, a phase-shifted analog beamformer is placed between N_f ($N_f < N_t$) RF chains and N_t transmit antennas, where the output of each RF chain is sent to all the transmit antennas.

A. Communication and sensing channel models

Let the reference point of the ULA be located at $(0, 0)$ and the coordinate of the n -th transmit antenna is $\mathbf{s}_n = (0, nd)$, where $n \in \mathcal{N}_t = \{1, \dots, N_t\}$. Consider a user located at r distance and θ angle from the center of the transmit ULA, so its coordinate is $\mathbf{r} = (r \cos \theta, r \sin \theta)$. Then, the distance from the n -th transmit antenna to this user can be calculated as

$$d_n(r, \theta) = \|\mathbf{r} - \mathbf{s}_n\| = \sqrt{r^2 + (nd)^2 - 2rnd \sin \theta}. \quad (1)$$

The resultant corresponding channel, \tilde{h}_n , can be modeled as $\tilde{h}_n = \tilde{\beta} e^{-j\frac{2\pi}{\lambda} d_n(r, \theta)}$, where $\tilde{\beta}$ is the free space path loss. In particular, $\tilde{\beta} = \frac{c}{4\pi f r}$, where f and c are the carrier frequency and speed of light, respectively. To capture the spherical wave characteristic in the NF, the second-order Taylor expansion can be utilized to approximate $d_n(r, \theta)$, i.e., $d_n(r, \theta) \approx r - \delta_n(r, \theta)$, where $\delta_n(r, \theta) = nd \sin \theta - (nd)^2 \cos^2 \theta / 2r$ [40]. Plugging it into \tilde{h}_n , the NF channel between the n -th transmit antenna and the user can be rewritten as $h_n = \beta e^{j\frac{2\pi}{\lambda} \delta_n(r, \theta)}$, where $\beta = \tilde{\beta} e^{-j\frac{2\pi}{\lambda} r}$. Then, the overall NF channel $\mathbf{h} \in \mathbb{C}^{N_t \times 1}$ between the transmit antennas and the user is

$$\mathbf{h} = \beta \left[e^{j\frac{2\pi}{\lambda} \delta_1(r, \theta)}, \dots, e^{j\frac{2\pi}{\lambda} \delta_{N_t}(r, \theta)} \right]^T = \beta \mathbf{a}(r, \theta). \quad (2)$$

where $\mathbf{a}(r, \theta)$ denotes the NF array response vector.

The general multi-path channel model comprises one line-of-sight (LoS) path and Q non-LoS (NLoS) paths induced by Q scatters. Let r_k ($r_{k,q}$) and θ_k ($\theta_{k,q}$) represent the distance and angle of user k (q -th scatter associated to user k). For this model, channel $\mathbf{h}_k \in \mathbb{C}^{N_t \times 1}$ can be characterized as

$$\mathbf{h}_k = \beta_k \mathbf{a}(r_k, \theta_k) + \sum_{q=1}^Q \beta_{k,q} \mathbf{a}(r_{k,q}, \theta_{k,q}). \quad (3)$$

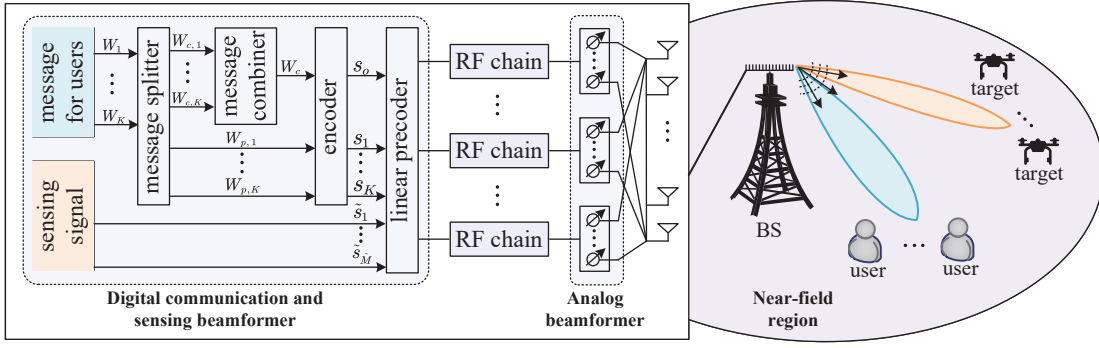


Fig. 1: The considered RSMA-aided NF-ISAC networks.

where $\beta_k = \tilde{\beta}_k e^{-j\frac{2\pi}{\lambda} r_k}$ and $\beta_{k,q} = \tilde{\beta}_{k,q} e^{-j\frac{2\pi}{\lambda} (r_{k,q} + \tilde{r}_{k,q})}$ are the complex channel gains of the LoS and the q -th NLoS components. $\tilde{r}_{k,q}$ is the distance between the k -th user and the q -th scatterer.

Target detecting depends on the echo signal received by the BS, so the BS needs to send probing signals and then gather echo signals. Using the array response vector in equation (2), round-trip sensing channel matrix $\mathbf{G}_m \in \mathbb{C}^{N_r \times N_t}$ of the m -th target can be modeled as

$$\mathbf{G}_m = \bar{\beta}_m \mathbf{b}(\bar{\mathbf{r}}_m, \bar{\boldsymbol{\theta}}_m) \mathbf{a}^T(\bar{\mathbf{r}}_m, \bar{\boldsymbol{\theta}}_m), \quad (4)$$

where $\bar{\beta}_m$ and $(\bar{\mathbf{r}}_m, \bar{\boldsymbol{\theta}}_m)$ are the round-trip complex channel gain and coordinate of the m -th target, respectively. $\mathbf{b}(\bar{\mathbf{r}}_m, \bar{\boldsymbol{\theta}}_m) \in \mathbb{C}^{N_r \times 1}$ and $\mathbf{a}(\bar{\mathbf{r}}_m, \bar{\boldsymbol{\theta}}_m) \in \mathbb{C}^{N_t \times 1}$ denote the receive and transmit NF array response vector, respectively.

B. Signal model, communication rate, and sensing rate

The BS utilizes downlink RSMA to serve communication users. Specifically, message W_k intended for the k -th user is split into a common part $W_{c,k}$ and a private part $W_{p,k}$ for $\forall k \in \mathcal{K}$. All common parts $\{W_{c,1}, \dots, W_{c,K}\}$ are combined and encoded into one common stream s_0 while the private parts $\{W_{p,1}, \dots, W_{p,K}\}$ are respectively encoded into private streams $\{s_1, \dots, s_K\}$. The unit-power signal stream vector at time index l can be expressed as $\mathbf{s}(l) = [s_0(l), s_1(l), \dots, s_K(l)]^T$, where $\forall l \in \mathcal{L} = \{1, \dots, L\}$ is the discrete-time index and L is the total transmit blocks within one coherent processing interval (CPI). The stream vector $\mathbf{s}(l)$ is linearly precoded by the hybrid beamformer $\mathbf{F}\mathbf{W} \in \mathbb{C}^{N_t \times (K+1)}$ to form communication beams, where $\mathbf{F} \in \mathbb{C}^{N_t \times N_f}$ is the analog beamforming matrix and $\mathbf{W} = [\mathbf{w}_0, \mathbf{w}_1, \dots, \mathbf{w}_K] \in \mathbb{C}^{N_f \times (K+1)}$ is the digital communication beamforming matrix. $\mathbf{w}_0 \in \mathbb{C}^{N_f \times 1}$ and $\mathbf{w}_k \in \mathbb{C}^{N_f \times 1}$ are the beamformers for the common stream and the k -th private stream, respectively. Additionally, to enhance sensing performance, the BS injects dedicated sensing beams. Similar to communication beams, these sensing streams are precoded by $\mathbf{F}\mathbf{V} \in \mathbb{C}^{N_t \times \tilde{M}}$ for $0 \leq \tilde{M} \leq N_f$ and then are superimposed with communications beams, where $\mathbf{V} = [\mathbf{v}_1, \dots, \mathbf{v}_{\tilde{M}}] \in \mathbb{C}^{N_f \times \tilde{M}}$. Note that, to have the maximum flexibility for ISAC beamforming design, a variable number of dedicated

sensing beams, denoted by \tilde{M} , are considered. Therefore, the transmitted signal at time index l can be written as

$$\mathbf{x}(l) = \mathbf{F}\mathbf{w}_0 s_0(l) + \sum_{k=1}^K \mathbf{F}\mathbf{w}_k s_k(l) + \sum_{m=1}^{\tilde{M}} \mathbf{F}\mathbf{v}_m \tilde{s}_m(l), \quad (5)$$

where $\tilde{s}_m(l)$ is the m -th dedicated sensing signal with unit-power at time index l . As such, the received signal at the k -th user can be written as

$$y_k(l) = \mathbf{h}_k^H \mathbf{x}(l) + n_k, \quad (6)$$

where $n_k \sim \mathcal{CN}(0, \sigma_k^2)$ denotes additional white Gaussian noise (AWGN) term. The average received power for the k -th user can be calculated by equation (7) as shown at the top of the next page.

To recover the desired message, the k -th user decodes the common stream by treating all private and dedicated sensing streams as noise. The signal-to-interference-plus-noise ratio (SINR) is $\gamma_{c,k} = S_{c,k} I_{c,k}^{-1}$. To ensure that all users can successfully decode the common stream, the common rate shall not exceed $R_c = \min_{\forall k} R_{c,k}$, where $R_{c,k} = \log(1 + \gamma_{c,k})$. Additionally, since all users share the common rate, $R_c = \sum_{k=1}^K C_{c,k}$, where $C_{c,k}$ is the portion of the common rate transmitting $W_{c,k}$. After removing the common stream via successive interference cancellation (SIC), the k -th user decodes the desired private stream by treating the residual streams as noise. The resultant SINR and achievable rate are $\gamma_{p,k} = S_{p,k} I_{p,k}^{-1}$ and $R_{p,k} = \log(1 + \gamma_{p,k})$, respectively. As such, the total transmit rate of user k is $R_k = C_{c,k} + R_{p,k}$.

Meanwhile, the detecting targets reflect $\mathbf{x}(l)$ to the BS, so the received echo signal at time index l is

$$\mathbf{y}(l) = \sum_{m=1}^{\tilde{M}} \sqrt{\alpha_m} \mathbf{G}_m \mathbf{x}(l) + \mathbf{G}_{SI} \mathbf{x}(l) + \mathbf{n}_0, \quad (8)$$

where α_m is the power reflection coefficient of the m -th target, $\mathbf{G}_{SI} \in \mathbb{C}^{N_r \times N_t}$ is self-interference channel, and $\mathbf{n}_0 \sim \mathcal{CN}(0, \sigma_0^2 \mathbf{I}_{N_r})$ is AWGN. This paper assumes the perfect self-interference cancellation. A similar assumption has been made in [33], [34]. After self-interference cancellation, the BS utilizes the receive filter $\mathbf{u}_m \in \mathbb{C}^{N_r \times 1}$ to acquire the

$$T_{c,k} = \underbrace{\left| \mathbf{h}_k^H \mathbf{F} \mathbf{w}_0 \right|^2}_{S_{c,k}} + \underbrace{\left| \mathbf{h}_k^H \mathbf{F} \mathbf{w}_k \right|^2}_{S_{p,k}} + \underbrace{\sum_{j=1, j \neq k}^K \left| \mathbf{h}_k^H \mathbf{F} \mathbf{w}_j \right|^2 + \sum_{m=1}^{\tilde{M}} \left| \mathbf{h}_k^H \mathbf{F} \mathbf{v}_m \right|^2}_{I_{p,k}} + \sigma^2. \quad (7)$$

$I_{c,k} = T_{p,k}$

desired reflected signal of the m -th target. The post-processed signal is thus given as

$$y(l) = \mathbf{u}_m^H \sum_{m=1}^M \sqrt{\alpha_m} \mathbf{G}_m \mathbf{s}(l) + \mathbf{u}_m^H \mathbf{n}_0. \quad (9)$$

The resultant detecting SINR of the m -th target is given as

$$\gamma_m = \frac{\alpha_m \mathbf{u}_m^H \mathbf{G}_m \mathbf{R} \mathbf{G}_m^H \mathbf{u}_m}{\mathbf{u}_m^H \left(\sum_{j=1, j \neq m}^M \alpha_j \mathbf{G}_j \mathbf{R} \mathbf{G}_j^H + \sigma_0^2 \mathbf{I}_{N_r} \right) \mathbf{u}_m}, \quad (10)$$

where $\mathbf{R} = \mathbb{E} [\mathbf{x}(l) \mathbf{x}^H(l)] = \mathbf{F} \mathbf{W} \mathbf{W}^H \mathbf{F}^H + \mathbf{F} \mathbf{V} \mathbf{V}^H \mathbf{F}^H$ is the covariance matrix. Consequently, the sensing rate of the m -th target is $\tilde{R}_m = \log(1 + \gamma_m)$.

C. Problem formulation

The transmit rate R_k and sensing rate \tilde{R}_m indicate that dedicated sensing beams incur harmful interference to users, while the communication beams can be repurposed to support target detection. In this context, a fundamental question arises: *i.e., does target detection need dedicated sensing beams? In other words, is NF target detection possible only using communication beams?* To address this issue, this paper aims to maximize the minimum communication rate among all users while meeting multi-target sensing rate constraints. This process requires the joint optimization of the number of dedicated sensing beams, analog beamformer, digital communication and sensing beamformers, receive filters, and common rate allocation. Therefore, this problem is formulated as

$$\max_{\tilde{M}, \mathbf{F}, \mathbf{W}, \mathbf{U}, \mathbf{V}, \mathbf{c}} \min_{\forall k} R_k, \quad (11a)$$

$$\text{s.t. } \|\mathbf{F} \mathbf{W}\|^2 + \|\mathbf{F} \mathbf{V}\|^2 \leq P_{\text{th}}, \quad (11b)$$

$$\tilde{R}_m \geq R_{\text{th}}, \quad \forall m, \quad (11c)$$

$$\sum_{k=1}^K C_{c,k} \leq R_c, \quad (11d)$$

$$C_{c,k} \geq 0, \quad \forall k, \quad (11e)$$

$$|\mathbf{F}_{i,j}| = 1, \quad 1 \leq i \leq N_t, \quad 1 \leq j \leq N_f, \quad (11f)$$

$$\|\mathbf{u}_m\|^2 = 1, \quad \forall m, \quad (11g)$$

$$1 \leq \tilde{M} \leq N_f, \quad (11h)$$

where $\mathbf{U} = [\mathbf{u}_1, \dots, \mathbf{u}_M]$ and $\mathbf{c} = [C_{c,1}, \dots, C_{c,K}]$. P_{th} and R_{th} denote the maximum transmit power and the sensing rate requirement thresholds, respectively. (11b) and (11c) are the transmit power and sensing performance constraints, respectively. (11d) and (11e) are the common rate allocation constraints. (11f) is the unit-modulus constraint of the analog beamformer while (11g) is the receive filter normalization constraint. (11h) is the number constraint of dedicated sensing beams.

Problem (11) appears elusive to optimally solve due to three technical challenges. First, the logarithmic function in R_k and \tilde{R}_m and minimum operator in R_c incur non-convexity and non-smoothness. Such problems are difficult to solve in both primal and dual domains since the duality gap is unknown. Second, the analog beamformer, digital beamformers, and receive filters are intricately coupled and cannot be separated, aggravating the solution difficulty. Third, the number of dedicated sensing beams is uncertain, complicating the optimization process. Consequently, the optimal solution is intractable.

III. DEDICATED SENSING BEAMS OR NOT?

This section aims to ascertain the number of dedicated sensing beams, eliminating its adverse impact in solving the problem (11). For this, the intuitive idea is to get the optimal solution and then check whether equation $\tilde{M} = 0$ holds. However, as discussed earlier, the optimal solution to problem (11) is mathematically intractable. An optimal solution reconstruction method is proposed to address this challenge, which rigorously meets $\tilde{M} = 0$. This reveals that dedicated sensing beams are not required for NF multi-target detection.

To eliminate the uncertainty incurred by \tilde{M} , we introduce auxiliary matrices $\tilde{\mathbf{W}}_k = \mathbf{w}_k \mathbf{w}_k^H$, $\tilde{\mathbf{V}} = \sum_{m=1}^{\tilde{M}} \mathbf{v}_m \mathbf{v}_m^H$, $\tilde{\mathbf{h}}_k = \mathbf{F}^H \mathbf{h}_k$, and $\tilde{\mathbf{H}}_k = \tilde{\mathbf{h}}_k \tilde{\mathbf{h}}_k^H$. As a result, the number of dedicated sensing beams is determined by the rank of $\tilde{\mathbf{V}}$, *i.e.*, $\tilde{M} = \text{rank}(\tilde{\mathbf{V}})$. Then, problem (11) can be recast as

$$\max_{\tilde{M}, \mathbf{F}, \tilde{\mathbf{W}}_k, \tilde{\mathbf{V}}, \mathbf{U}, \mathbf{c}} \min_{\forall k} R_k, \quad (12a)$$

$$\text{s.t. } \sum_{k=0}^K \text{Tr}(\mathbf{F}^H \mathbf{F} \tilde{\mathbf{W}}_k) + \text{Tr}(\mathbf{F}^H \mathbf{F} \tilde{\mathbf{V}}) \leq P_{\text{th}}, \quad (12b)$$

$$\tilde{\mathbf{W}}_k \succeq \mathbf{0}, \quad \tilde{\mathbf{V}} \succeq \mathbf{0}, \quad \forall k \in \mathcal{K}_1, \quad (12c)$$

$$\text{rank}(\tilde{\mathbf{W}}_k) = 1, \quad \forall k \in \mathcal{K}_1, \quad (12d)$$

$$(11c) - (11h). \quad (12e)$$

where $\mathcal{K}_1 = \{0, 1, \dots, K\}$. Note that equation (7) should be substituted by equation (13) shown at the top of the next page in calculating the communication rate. Meanwhile, \mathbf{R} should be updated to $\mathbf{R} = \sum_{k=0}^K \mathbf{F} \tilde{\mathbf{W}}_k \mathbf{F}^H + \mathbf{F} \tilde{\mathbf{V}} \mathbf{F}^H$. The non-convex rank-one constraint and fractional SINR make the optimization problem intractable for direct solutions. Therefore, the specific value of the optimal solution cannot be determined, but there should be at least one optimal solution. Let $\mathcal{Q}_1^* = \{\mathbf{F}^*, \tilde{\mathbf{W}}_k^*, \tilde{\mathbf{V}}^*, \mathbf{U}^*, \mathbf{c}^*\}$ denote the optimal solution, but $\text{rank}(\tilde{\mathbf{V}}^*)$ is difficult to be determined analytically. To counter this challenge, Proposition 1, proved in Appendix A, constructs an equivalent optimal rank-zero solution but may violate $\text{rank}(\tilde{\mathbf{W}}_k) = 1$.

$$T_{c,k} = \underbrace{\text{Tr}(\mathbf{H}_k \tilde{\mathbf{W}}_0)}_{S_{c,k}} + \underbrace{\text{Tr}(\mathbf{H}_k \tilde{\mathbf{W}}_k)}_{S_{p,k}} + \underbrace{\sum_{j=1, j \neq k}^K \text{Tr}(\mathbf{H}_k \tilde{\mathbf{W}}_j) + \text{Tr}(\mathbf{H}_k \tilde{\mathbf{V}})}_{I_{p,k}} + \sigma^2. \quad (13)$$

Proposition 1: If rank-one constraint (12d) is temporarily relaxed, one can always construct other solution $\mathcal{Q}_2 = \{\mathbf{F}^*, \tilde{\mathbf{W}}_k, \tilde{\mathbf{V}}, \mathbf{U}^*, \mathbf{c}^*\}$ that guarantees $E(\mathcal{Q}_2) \geq E(\mathcal{Q}_1^*)$, where $E(\mathcal{Q})$ denotes the objective value achieved by the solution \mathcal{Q} and

$$\hat{\mathbf{W}}_k = \tilde{\mathbf{W}}_k^* + \delta_k \tilde{\mathbf{V}}^* \text{ and } \hat{\mathbf{V}} = \mathbf{0}. \quad (14)$$

In equation (14), the arbitrary weighted coefficients must meet $\sum_{k=0}^K \delta_k = 1$ and $\delta_k \geq 0$.

Proposition 1 reveals that removing dedicated sensing beams will not hinder the sensing rate when neglecting the rank-one constraints (12d). However, the constructed digital communication beamformers may not be rank-one, *i.e.*, $\tilde{\mathbf{W}}_k \geq 1$, so the conclusion in Proposition 1 cannot apply to the problem (12). Proposition 2, proved in Appendix B, creates a feasible rank-one solution from the high-rank solution $\tilde{\mathbf{W}}_k$ to address this issue.

Proposition 2: Keeping other variable blocks unchanged, a feasible rank-one solution $\{\bar{\mathbf{W}}_k = \bar{\mathbf{w}}_k \bar{\mathbf{w}}_k^H\}$ can be constructed for problem (12), which yields the same performance with high-rank solution $\{\tilde{\mathbf{W}}_k\}$, *i.e.*, $E(\mathcal{Q}_3) = E(\mathcal{Q}_2)$, where $\mathcal{Q}_3 = \{\mathbf{F}^*, \bar{\mathbf{W}}_k, \tilde{\mathbf{V}}, \mathbf{U}^*, \mathbf{c}^*\}$.

Proposition 2 proves that \mathcal{Q}_3 can satisfy all of the constraints in problem (12). Combining Proposition 1 and Proposition 2 yields

$$E(\mathcal{Q}_3) = E(\mathcal{Q}_2) \geq E(\mathcal{Q}_1^*). \quad (15)$$

Equation (15) shows that \mathcal{Q}_3 can yield the same performance with \mathcal{Q}_1^* at least. Since \mathcal{Q}_1^* has produced the maximal objective value, it is thus deduced that the equation sign holds and \mathcal{Q}_3 is an optimal solution. Therefore, there exists an optimal solution making $\mathbf{V} = \mathbf{0}$, which indicates the non-necessity of dedicated sensing beams in NF multi-target detection, *i.e.*, $\tilde{M}^* = 0$.

IV. ALGORITHM AND ANALYSIS

This section focuses on optimizing the analog beamformer, digital communication beamformers, receive filters, and common rate allocation, given that dedicated sensing beams have been shown to be unnecessary. To optimize the system, the PDD, WMMSE, and quadratic transform approaches are leveraged to design a PDD-based double-loop algorithm. Specifically, the PDD method is used to reformulate the problem (11) into a more manageable form. The WMMSE and quadratic transform methods are then applied to recast communication and sensing rates into easily optimized constraints. Additionally, the algorithm is summarized, and its convergence and complexity are discussed.

To proceed, we introduce an auxiliary matrix $\mathbf{P} = [\mathbf{p}_0, \dots, \mathbf{p}_k] \in \mathbb{C}^{N_t \times (K+1)}$, which meets $\mathbf{p}_k = \mathbf{F}\mathbf{w}_k$ for

$\forall k \in \mathcal{K}_1$. Plugging $\tilde{M}^* = 0$ and $\mathbf{p}_k = \mathbf{F}\mathbf{w}_k$ into equation (7), the received power by the k -th user can be adjusted to

$$T_{c,k} = \underbrace{|\mathbf{h}_k^H \mathbf{p}_0|^2}_{S_{c,k}} + \underbrace{|\mathbf{h}_k^H \mathbf{p}_k|^2}_{S_{p,k}} + \underbrace{\sum_{j=1, j \neq k}^K |\mathbf{h}_k^H \mathbf{p}_j|^2}_{I_{p,k}} + \sigma^2, \quad (16)$$

which is used to recalculate the common and private rates. Similarly, the covariance matrix should be updated to $\mathbf{R} = \mathbf{P}\mathbf{P}^H$. We introduce a non-negative auxiliary variable R_s to attack the non-smoothness incurred by (11a). Consequently, the resultant new problem is

$$\max_{\mathcal{Q}} R_s, \quad (17a)$$

$$\text{s.t. } \mathbf{P} = \mathbf{F}\mathbf{W}, \quad (17b)$$

$$\|\mathbf{P}\|^2 \leq P_{\text{th}}, \quad (17c)$$

$$R_k \geq R_s, \quad \forall k, \quad (17d)$$

$$(11c) - (11g). \quad (17e)$$

where $\mathcal{Q} = \{\mathbf{P}, \mathbf{F}, \mathbf{W}, \mathbf{U}, \mathbf{c}, R_s\}$ collects all optimization variables. The equality constraint (17a) still hinders the optimization process. To address this issue, the PDD approach [41] is adopted. Specifically, it transfers constraint (17b) into the objective function by introducing the Lagrangian dual variable and penalty parameter, creating a double-loop iterative problem. The outer loop updates the Lagrangian dual matrix and the penalty parameter. Readers are referred to [41] for more details about updating rules. The inner loop solves the augmented Lagrangian (AL) problem. By introducing Lagrangian dual matrix \mathbf{D} and penalty parameter ρ , the AL problem is formulated as

$$\max_{\mathcal{Q}} R_s - \mathbf{D}^H (\mathbf{P} - \mathbf{F}\mathbf{W}) - \frac{1}{2\rho} \|\mathbf{P} - \mathbf{F}\mathbf{W}\|^2, \quad (18a)$$

$$\text{s.t. } (11c) - (11g), (17c), (17d). \quad (18b)$$

Alg. 1 summarizes the proposed PDD-based double-loop algorithm framework. Given the known dual matrix and penalty parameter, solving problem (18) appears intractable. However, the constraints in problem (18) are separable. This observation motivates us to divide variables into several blocks and optimize each block alternately. The optimization of each block is elaborated next.

A. Subproblem with respect to $\{\mathbf{U}\}$

With fixed auxiliary matrix \mathbf{P} , optimizing \mathbf{u}_m for detecting the m -th target will not impact other targets. Therefore, problem (18) can be divided into M independent subproblems. In each subproblem, \mathbf{u}_m is optimized to enhance the

Algorithm 1 PDD-based framework for solving problem (17)

- 1: Initialize $\mathbf{F}^{(0)}$, $\mathbf{W}^{(0)}$, $\mathbf{D}^{(0)}$, $\rho^{(0)}$, and $\psi^{(0)}$, set iteration index $n = 1$ and the maximum tolerance ξ_1 .
 - 2: **while** not convergent **do**
 - 3: Solving problem (18) to obtain $\mathbf{P}^{(n)}$, $\mathbf{F}^{(n)}$, and $\mathbf{W}^{(n)}$ via Alg. 2.
 - 4: **if** $\|\mathbf{P}^{(n)} - \mathbf{F}^{(n)}\mathbf{W}^{(n)}\|_\infty \leq \psi^{(n-1)}$ **then**
 - 5: Update $\mathbf{D}^{(n)} = \mathbf{D}^{(n-1)} + \frac{1}{\rho^{(n)}} (\mathbf{P}^{(n)} - \mathbf{F}^{(n)}\mathbf{W}^{(n)})$.
 - 6: Keep penalty factor unchanged, i.e., $\rho^{(n)} = \rho^{(n-1)}$.
 - 7: **else**
 - 8: Update $\rho^{(n)} = \mu\rho^{(n-1)}$, where $0 < \mu < 1$.
 - 9: Keep Lagrangian dual matrix \mathbf{D} unchanged, i.e., $\mathbf{D}^{(n)} = \mathbf{D}^{(n-1)}$.
 - 10: **end if**
 - 11: Update $\psi^{(n)} = 0.9\|\mathbf{P}^{(n)} - \mathbf{F}^{(n)}\mathbf{W}^{(n)}\|_\infty$ and $n = n + 1$.
 - 12: **end while**
 - 13: Output the maximized minimum sensing rate.
-

sensing SINR for the m -th target, which yields the following optimization problem

$$\max_{\mathbf{u}_m} \frac{\alpha_m \mathbf{u}_m^H \mathbf{G}_m \mathbf{R} \mathbf{G}_m^H \mathbf{u}_m}{\mathbf{u}_m^H \mathbf{Q}_m \mathbf{u}_m} \quad (19a)$$

$$\text{s.t. } \|\mathbf{u}_m\|^2 = 1, \quad (19b)$$

where $\mathbf{Q}_m = \sum_{j=1, j \neq m}^M \alpha_j \mathbf{G}_j \mathbf{R} \mathbf{G}_j^H + \sigma_0^2 \mathbf{I}_{N_r}$. Problem (19) is a generalized Rayleigh quotient problem [16], and its optimal solution is

$$\mathbf{u}_m^* = \mathbf{v}_{\max}(\mathbf{Q}_m^{-1} \mathbf{G}_m \mathbf{R} \mathbf{G}_m^H), \quad \forall m, \quad (20)$$

where $\mathbf{v}_{\max}(\mathbf{A})$ denotes the eigenvector corresponding to the maximum eigenvalue of matrix \mathbf{A} .

B. Subproblem with respect to $\{\mathbf{P}, \mathbf{c}, R_s\}$

With fixed analog beamformer \mathbf{F} , digital beamformer \mathbf{W} , and receive filter \mathbf{U} , problem (18) can be simplified as

$$\max_{\mathbf{P}, \mathbf{c}, R_s} R_s - \mathbf{D}^H (\mathbf{P} - \mathbf{F}\mathbf{W}) - \frac{1}{2\rho} \|\mathbf{P} - \mathbf{F}\mathbf{W}\|^2, \quad (21a)$$

$$\text{s.t. } (11c), (11d), (11e), (17c), (17d). \quad (21b)$$

1) *WMMSE for common and private rates*: Problem (21) involves the fractional SINR and coupled auxiliary variables, which is difficult to solve directly. The WMMSE approach is particularly effective in dealing with logarithmic transmit rate expressions by introducing equalizers [42]. Thus, it is employed to recast common rate $R_{c,k}$ and private rate $R_{p,k}$. Specifically, the k -th user utilizes equalizer $\omega_{c,k}$ to the received signal, realizing the estimation of s_0 , denoted by $\hat{s}_{c,k} = \omega_{c,k} y_k$, where time index l is dropped for brevity. After removing the common stream via SIC, equalizer $\omega_{p,k}$ is applied to obtain an estimate of \hat{s}_k given by $\hat{s}_k = \omega_{p,k} (y_k - \mathbf{h}_k^H \mathbf{p}_0 s_0)$. Subsequently, the mean-squared errors (MSEs) of common and private streams, defined respectively

as $\delta_{c,k} = \mathbb{E} \left\{ |\hat{s}_{c,k} - s_0|^2 \right\}$ and $\delta_{p,k} = \mathbb{E} \left\{ |\hat{s}_k - s_k|^2 \right\}$, are given as

$$\delta_{c,k} = |\omega_{c,k}|^2 T_{c,k} - 2\text{Re}(\omega_{c,k} \mathbf{h}_k^H \mathbf{p}_0) + 1, \quad (22a)$$

$$\delta_{p,k} = |\omega_{p,k}|^2 T_{p,k} - 2\text{Re}(\omega_{p,k} \mathbf{h}_k^H \mathbf{p}_k) + 1. \quad (22b)$$

By solving $\frac{\partial \delta_{c,k}}{\partial \omega_{c,k}} = 0$ and $\frac{\partial \delta_{p,k}}{\partial \omega_{p,k}} = 0$, the optimum minimum MSE (MMSE) equalizers are respectively expressed as

$$\omega_{c,k}^{\text{MMSE}} = \mathbf{p}_0^H \mathbf{h}_k T_{c,k}^{-1} \quad \text{and} \quad \omega_{p,k}^{\text{MMSE}} = \mathbf{p}_k^H \mathbf{h}_k T_{p,k}^{-1}. \quad (23)$$

Substituting (23) into (22), the resulting MMSEs are written as

$$\delta_{c,k}^{\text{MMSE}} = \min_{\omega_{c,k}} \delta_{c,k} = T_{c,k}^{-1} I_{c,k}, \quad (24a)$$

$$\delta_{p,k}^{\text{MMSE}} = \min_{\omega_{p,k}} \delta_{p,k} = T_{p,k}^{-1} I_{p,k}. \quad (24b)$$

The MMSEs are related to the SINRs such that $\gamma_{c,k} = 1/\delta_{c,k}^{\text{MMSE}} - 1$ and $\gamma_{p,k} = 1/\delta_{p,k}^{\text{MMSE}} - 1$, from which the transmit rate can be expressed as $R_{c,k} = -\log(\delta_{c,k}^{\text{MMSE}})$ and $R_{p,k} = -\log(\delta_{p,k}^{\text{MMSE}})$, respectively.

Next, the augmented weighted MSEs (WMSEs) are defined as $\beta_{c,k} = \eta_{c,k} \delta_{c,k} - \log(\eta_{c,k})$ and $\beta_{p,k} = \eta_{p,k} \delta_{p,k} - \log(\eta_{p,k})$, where $\eta_{c,k}$ and $\eta_{p,k}$ are the weights associated with the k -th user's MSEs. By taking the equalizers and weights as optimization variables, the rate-WMMSE relationship is established as

$$\beta_{c,k}^{\text{MMSE}} = \min_{\eta_{c,k}, \omega_{c,k}} \beta_{c,k} = \tau - R_{c,k}, \quad (25a)$$

$$\beta_{p,k}^{\text{MMSE}} = \min_{\eta_{p,k}, \omega_{p,k}} \beta_{p,k} = \tau - R_{p,k}, \quad (25b)$$

where $\tau = 1/\ln 2 + \log(\ln 2)$. By setting $\frac{\partial \beta_{c,k}}{\partial \omega_{c,k}} = 0$ and $\frac{\partial \beta_{p,k}}{\partial \omega_{p,k}} = 0$, the optimal equalizers become $\omega_{c,k}^* = \omega_{c,k}^{\text{MMSE}}$ and $\omega_{p,k}^* = \omega_{p,k}^{\text{MMSE}}$. Similarly, the optimal weights can be derived as follows

$$\eta_{c,k}^* = (\delta_{c,k}^{\text{MMSE}} \ln 2)^{-1} \quad \text{and} \quad \eta_{p,k}^* = (\delta_{p,k}^{\text{MMSE}} \ln 2)^{-1}. \quad (26)$$

By closely examining each WMSE, it is convex in each variable when the other two are specified.

2) *Quadratic transform for sensing rate*: The WMMSE approach cannot convert the sensing rate, necessitating an alternative solution. Here, the quadratic transform approach is employed to construct an accurate surrogate for the sensing rate, as first proposed in [43]. Proposition 3 is motivated by Theorem 2 in [43].

Proposition 3: After introducing our constructed surrogate function $f(\mathbf{x}, \mathbf{P}) = 2\text{Re}(\mathbf{x}^H \mathbf{s}(\mathbf{P}) - \mathbf{x}^H I(\mathbf{P}) \mathbf{x})$ for any $\mathbf{s}(\mathbf{P}) \in \mathbb{C}^{N_t \times 1}$ and $I(\mathbf{P}) > 0$, we can derive

$$\frac{(\mathbf{s}(\mathbf{P}))^H \mathbf{s}(\mathbf{P})}{I(\mathbf{P})} = \max_{\mathbf{x}} f(\mathbf{x}, \mathbf{P}) \quad (27)$$

and the optimal solution to the right-hand of equation (27) is $\mathbf{x}^* = \frac{\mathbf{s}(\mathbf{P})}{I(\mathbf{P})}$.

Engaging Proposition 3 to construct the surrogate for the sensing SINR yields

$$f_m(\mathbf{x}_m, \mathbf{P}) = 2\alpha_m \text{Re}(\mathbf{x}_m^H \mathbf{u}_m^H \mathbf{Q}_m) - \mathbf{x}_m^H \mathbf{u}_m^H \mathbf{Q}_m \mathbf{u}_m \mathbf{x}_m, \quad (28)$$

where \mathbf{x}_m is the introduced auxiliary variable. Using the rate-WMMSE relationship (25) and constructed surrogate (28) for sensing SINR, one can recast (21) as

$$\max_{\hat{\mathcal{Q}}_1, \hat{\mathcal{Q}}_2} R_s - \mathbf{D}^H (\mathbf{P} - \mathbf{F}\mathbf{W}) - \frac{1}{2\rho} \|\mathbf{P} - \mathbf{F}\mathbf{W}\|^2, \quad (29a)$$

$$\text{s.t. } \sum_{k=1}^K C_{c,k} + \min_{\eta_{c,k}, \omega_{c,k}} \beta_{c,k} \leq \tau, \quad \forall k, \quad (29b)$$

$$C_{c,k} - \min_{\eta_{p,k}, \omega_{p,k}} \beta_{p,k} \geq R_s - \tau, \quad \forall k, \quad (29c)$$

$$\log \left(1 + \max_{\mathbf{x}_m} f_m(\mathbf{x}_m, \mathbf{P}) \right) \geq R_{\text{th}}, \quad \forall m, \quad (29d)$$

$$(11e), (17c). \quad (29e)$$

$\hat{\mathcal{Q}}_1$ and $\hat{\mathcal{Q}}_2$ collect respectively the intrinsic variables and introduced auxiliary variables, *i.e.*, $\hat{\mathcal{Q}}_1 = \{\mathbf{P}, \mathbf{c}, R_s\}$ and $\hat{\mathcal{Q}}_2 = \{\eta_{c,k}, \omega_{c,k}, \eta_{p,k}, \omega_{p,k}, \mathbf{x}_m\}$. The non-trivial coupling between $\hat{\mathcal{Q}}_1$ and $\hat{\mathcal{Q}}_2$ makes problem (29) difficult to solve directly. However, observe that problem (29) becomes convex upon fixing introduced auxiliary variable $\hat{\mathcal{Q}}_2$. Driven by this observation, we consider optimizing $\hat{\mathcal{Q}}_i$ while keeping $\hat{\mathcal{Q}}_j$ at its previous value and vice versa, where $\forall i, j \in \{1, 2\}$ and $j \neq i$. Specifically, the intrinsic variables are solved via convex optimization solvers while the optimal auxiliary variables with closed-form expressions are derived according to (23), (26), and (30). That is,

$$\mathbf{x}_m^* = \mathbf{u}_m^H \mathbf{q}_m, \quad \forall m, \quad (30)$$

which is derived from Proposition 3.

C. Subproblem with respect to $\{\mathbf{F}, \mathbf{W}\}$

The variables \mathbf{F} and \mathbf{W} only appear in the last two-term of the objective function, so problem (18) reduces to

$$\min_{\mathbf{F}, \mathbf{W}} \mathbf{D}^H (\mathbf{P} - \mathbf{F}\mathbf{W}) + \frac{1}{2\rho} \|\mathbf{P} - \mathbf{F}\mathbf{W}\|^2, \quad (31a)$$

$$\text{s.t. } (11f). \quad (31b)$$

To streamline the optimization process, (31a) is equivalently transformed to $\frac{1}{2\rho} \|\mathbf{P} - \mathbf{F}\mathbf{W} + \rho\mathbf{D}\|^2 + \rho^2\mathbf{D}^2$. Omitting constant $\rho^2\mathbf{D}^2$ and positive coefficient $\frac{1}{2\rho}$, problem (31) is recast to

$$\min_{\mathbf{F}, \mathbf{W}} \|\mathbf{P} - \mathbf{F}\mathbf{W} + \rho\mathbf{D}\|^2, \quad (32a)$$

$$\text{s.t. } (11f). \quad (32b)$$

As (31) is a highly coupled quadratic problem, optimizing analog and digital beamformers alternately is the solution.

1) *Digital beamformer optimization:* With fixed \mathbf{F} , problem (31) is simplified as $\min_{\mathbf{W}} \|\mathbf{P} - \mathbf{F}\mathbf{W} + \rho\mathbf{D}\|^2$, which is a quadratic function. By solving $\frac{\partial \|\mathbf{P} - \mathbf{F}\mathbf{W} + \rho\mathbf{D}\|^2}{\partial \mathbf{W}} = 0$, the optimal solution is found as

$$\mathbf{W}^* = (\mathbf{F}^H \mathbf{F})^{-1} \mathbf{F}^H (\mathbf{P} + \rho\mathbf{D}). \quad (33)$$

2) *Analog beamformer optimization:* With fixed \mathbf{W} , problem (31) can be simplified as

$$\min_{\mathbf{F}} \text{Tr}(\mathbf{F}^H \mathbf{F} \mathbf{Y}) - 2\text{Re}(\text{Tr}(\mathbf{F}^H \mathbf{Z})), \quad (34a)$$

$$\text{s.t. } |\mathbf{F}_{i,j}| = 1, \quad 1 \leq i \leq N_t, \quad 1 \leq j \leq N_f, \quad (34b)$$

Algorithm 2 Alternating algorithm for solving problem (18)

- 1: Set $\mathbf{F}^{(1)} = \mathbf{F}^{(n-1)}$ and $\mathbf{W}^{(1)} = \mathbf{W}^{(n-1)}$, set iteration index $i = 1$, and the maximum tolerance $\xi = 10^{-3}$.
 - 2: **while** not convergent **do**
 - 3: Update $\mathbf{U}^{(i)}$ according to equation (20).
 - 4: Update $\omega_{c,k}^{(i)}$ and $\omega_{p,k}^{(i)}$ according to equation (23).
 - 5: Update $\eta_{c,k}^{(i)}$ and $\eta_{p,k}^{(i)}$ according to equation (26).
 - 6: Update $\mathbf{x}_m^{(i)}$ according to equation (30).
 - 7: Obtain optimal $\mathbf{P}^{(i)}$ and $\mathbf{c}^{(i)}$ by solving problem (29).
 - 8: Update $\mathbf{W}^{(i+1)}$ according to equation (33).
 - 9: Update $\mathbf{F}^{(i+1)}$ according to equation (36).
 - 10: Update iteration index $i = i + 1$.
 - 11: **end while**
 - 12: Output $\mathbf{P}^{(n)}$, $\mathbf{F}^{(n)}$, and $\mathbf{W}^{(n)}$.
-

where $\mathbf{Y} = \mathbf{W}\mathbf{W}^H$ and $\mathbf{Z} = (\mathbf{P} + \rho\mathbf{D})\mathbf{W}^H$. The elements of \mathbf{F} are separated in unit-modulus constraint (34b), which motivates us to optimize \mathbf{F} by one element at a time. Consequently, the optimization problem for $\mathbf{F}_{i,j}$ reduces to

$$\min_{\mathbf{F}_{i,j}} \phi_{i,j} |\mathbf{F}_{i,j}|^2 - 2\text{Re}(\chi_{i,j} \mathbf{F}_{i,j}), \quad (35a)$$

$$\text{s.t. } (34b). \quad (35b)$$

where $\phi_{i,j}$ and $\chi_{i,j}$ are real and complex constant coefficients determined by the elements of \mathbf{F} except for $\mathbf{F}_{i,j}$, respectively. Under unit-modulus constraint (34b), optimal $\mathbf{F}_{i,j}$ can be obtained by

$$\mathbf{F}_{i,j}^* = \frac{\chi_{i,j}^H}{|\chi_{i,j}|}. \quad (36)$$

At present, coefficient $\chi_{i,j}$ in (35) remains unknown. However, objective functions (34) and (35) have the same partial derivatives with respect to $\mathbf{F}_{i,j}$, so we can derive

$$\mathbf{X}_{i,j} - \mathbf{Z}_{i,j} = \phi_{i,j} \tilde{\mathbf{F}}_{i,j} - \chi_{i,j}, \quad (37)$$

where $\mathbf{X} = \tilde{\mathbf{F}}\mathbf{Y}$ and $\tilde{\mathbf{F}}$ denotes that the optimized solution of \mathbf{F} in the previous iteration. Moreover, expanding $\tilde{\mathbf{F}}\mathbf{Y}$ yields $\phi_{i,j} \tilde{\mathbf{F}}_{i,j} = \tilde{\mathbf{F}}_{i,j} \mathbf{Y}_{j,j}$, so we have

$$\chi_{i,j} = \mathbf{Z}_{i,j} - \mathbf{X}_{i,j} + \tilde{\mathbf{F}}_{i,j} \mathbf{Y}_{j,j}. \quad (38)$$

The proposed alternating algorithm for problem (18) is summarized in Alg. 2, where receive filters, digital beamformer, analog beamformer, and introduced auxiliary variables are iteratively updated till convergence.

D. Convergence and Complexity Analysis

The proposed solution for (17) is summarized in Alg. 1. Next, its critical properties (*i.e.*, convergence, optimality, and complexity) are discussed.

- *Convergence:* Starting from any feasible initial point, the algorithm always yields globally optimal solutions, ensuring it can locate the final feasible point. As a result, the objective value remains stable or improves with each iteration. Additionally, since the sensing rate is an upper bound, the algorithm converges to a stationary point within a finite number of iterations.

- **Complexity:** The main computational load in each iteration stems from Alg. 2. In Alg. 2, optimal \mathbf{P} and \mathbf{c} are solved via CVX while the remaining variables are updated by the closed-form solutions. The complexity using the interior point method is $\mathcal{O}(N_v^{3.5})$, where N_v is the number of variables. Thus, the complexity of updating \mathbf{P} and \mathbf{c} is in order of $\mathcal{O}((K+1)^{3.5}(N_t+1)^{3.5})$. The complexity of updating other variables stems from the matrix inversion, multiplication, and eigenvalue decomposition. For two matrices $\mathbf{W}_1 \in \mathbb{C}^{A_1 \times A_2}$ and $\mathbf{W}_2 \in \mathbb{C}^{A_2 \times A_3}$, the complexity of $\mathbf{W}_1 \mathbf{W}_2$ is $\mathcal{O}(A_1 A_2 A_3)$. For matrix $\mathbf{W}_3 \in \mathbb{C}^{A_4 \times A_4}$, the complexity inversion and eigenvalue decomposition are $\mathcal{O}(A_4^3)$. Therefore, the complexity from line 3 to line 9 (excluding line 7) are in order of $\mathcal{O}(M(N_r^3 + N_r^2 N_t + N_r N_t^2))$, $\mathcal{O}(K N_t^2)$, $\mathcal{O}(K N_t^2)$, $\mathcal{O}(K(N_r N_t + N_t^2))$, $\mathcal{O}(N_f^2 N_t + N_f^3 + N_f N_T(K+1))$, and $\mathcal{O}(N_t N_f(K+1))$, respectively. By retaining the higher-order terms, the per-iteration computational complexity of Alg. 2 is $\mathcal{O}(M(N_r^3 + N_r^2 N_t + N_r N_t^2) + (K+1)^{3.5}(N_t+1)^{3.5})$.

V. SIMULATION RESULT

Numerical results evaluate our proposed transmit scheme and algorithm. Unless stated otherwise, simulation parameters are as follows: The BS has $N_t = 64$ and $N_r = 64$ antennas operating at $f_c = 30$ GHz. The antenna array aperture is set to $D_t = D_r = 0.5$ m, resulting in a Rayleigh distance of around 50 m. The RF chains and scatters associated with each communication user are set to $N_f = 8$ and $Q = 2$, respectively. Scatters for communication links are randomly generated within the distance from 20 m to 30 m. $K = 6$ communication users and $M = 4$ sensing targets are randomly distributed throughout the NF region. The maximum transmit power at the BS and background noise power are $P_{\text{th}} = 30$ dBm and $\sigma^2 = -80$ dBm, respectively. The sensing rate requirement of each target is $R_{\text{th}} = 6$ bps/Hz. These parameters are primarily sourced from [10], [32], [34].

Each point is averaged over 100 independent channel realizations. The proposed transmit scheme (labeled as **RSMA-HB, near**) is compared against four baselines to assess its performance comprehensively. They are described next.

- **RSMA-FD, near:** Each antenna connects to a dedicated RF chain, enabling full-dimensional beamforming. This fully digital antenna architecture is an upper performance bound [44] for the proposed architecture, which adopts an analog and digital beamforming hybrid. The analog beamformer is constrained by unit modulus, e.g., (11f). In contrast, the full digital beamforming benchmark does not have this constraint, resulting in a larger feasible region.
- **SDMA-HB, near:** Each user's message is encoded to a private stream while each receiver decodes its desired stream by treating other streams as noise. Thus, this baseline disables the common stream, i.e., $\mathbf{w}_0 = \mathbf{0}$.
- **RSMA-Com, near:** This benchmark neglects the requirement for multi-target detection, i.e., $R_{\text{th}} = 0$. This

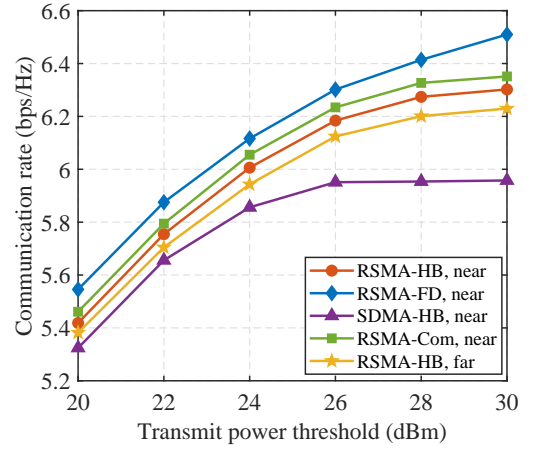


Fig. 2: Max-min communication rate versus transmit power.

reveals the impact of using communication beams to detect targets on communication performance.

- **RSMA-HB, far:** This one adopts the FF channel model to confirm the benefits of NF beamforming. For a fair comparison, all parameters are identical to the NF counterpart except for the array response vector. In FF channels, the array response vector in equation (2) is updated to

$$\mathbf{a}_{\text{far}}(\theta) = \left[e^{j\frac{2\pi}{\lambda} d \sin \theta}, \dots, e^{j\frac{2\pi}{\lambda} N d \sin \theta} \right]^T. \quad (39)$$

Figure 2 shows the max-min communication rate versus transmit power, highlighting four key advantages of the proposed scheme over competing benchmarks:

- 1) **Effective Interference Management:** While the communication rate increases with transmit power across all schemes, SDMA stagnates at $P_{\text{th}} \geq 26$ dBm due to excessive interference. In contrast, the gap between RSMA and SDMA widens, demonstrating RSMA's superior interference handling.
- 2) **NF Beamforming Superiority:** The proposed NF scheme outperforms the FF system by leveraging NF beamforming to focus energy on specific points and minimize inter-user interference through reduced leakage.
- 3) **Minimal Impact of Sensing Constraints:** Meeting the sensing rate of 6 bps/Hz reduces the communication rate by only 0.05 bps/Hz, highlighting the efficiency of the RSMA-enabled NF-ISAC design.
- 4) **Comparable to Full Digital Beamforming:** Full digital beamforming achieves a communication rate gain of 0.05 bps/Hz at $P_{\text{th}} \leq 28$ dBm and 0.13 bps/Hz at $P_{\text{th}} = 30$ dBm over proposed hybrid beamforming. This demonstrates the proposed scheme's ability to perform near the level of fully digital beamforming.

Fig. 3 shows the max-min communication rate versus the number of RF chains. From the figure, our proposed hybrid beamforming algorithm can achieve a comparable communication rate to the full digital beamforming when $N_f > K$. This is because that digital beamforming can create sufficient spatial Degrees of Freedom (DoF) to neutralize interference. However, when the number of RF chains decreases, data streams exceed the DoF created through classical digital beamforming,

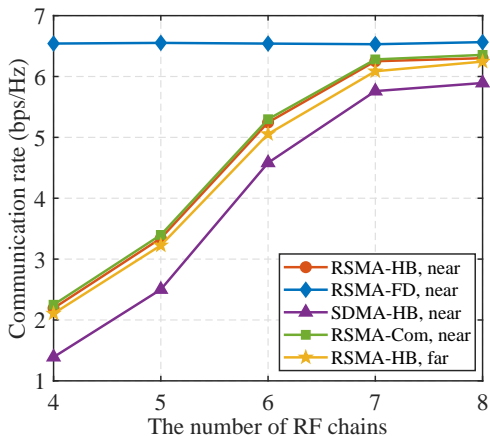


Fig. 3: Max-min communication rate versus the number of RF chains.

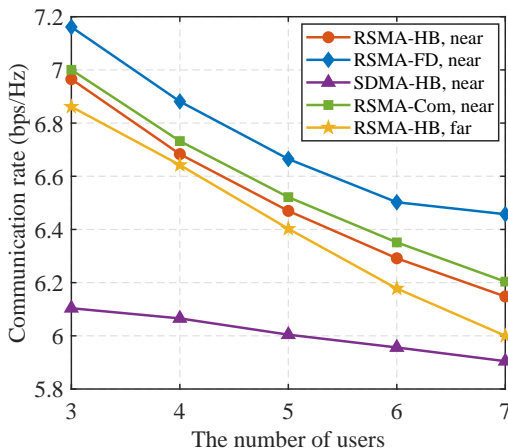


Fig. 4: Max-min communication rate versus the number of users.

degrading the communication performance. Therefore, the performance gap between hybrid beamforming and full digital beamforming becomes clearer when $N_f < K$. However, under an identical number of RF chains, our proposed transmit scheme always performs close to communication-only networks and surpasses SDMA and FF-ISAC.

Fig. 4 presents the max-min communication rate versus the number of users. As anticipated, all approaches reduce the max-min communication rate as more users are scheduled. Moreover, the performance gap between RSMA and SDMA schemes gradually narrows. This phenomenon happens since all users are required to decode the common stream. However, the common rate depends on the user with the poorest worst channel quality and is shared by all communication users. The gap between NF- and FF-ISACs becomes more obvious. This is because spherical-wave propagation can distinguish users with similar angular directions and then focus the beam energy on a specific point, which helps neutralize intra-user interference.

Fig. 5 investigates the impact of the number of targets on the communication rate. All transmit schemes degrade the max-min communication rate as the number of targets

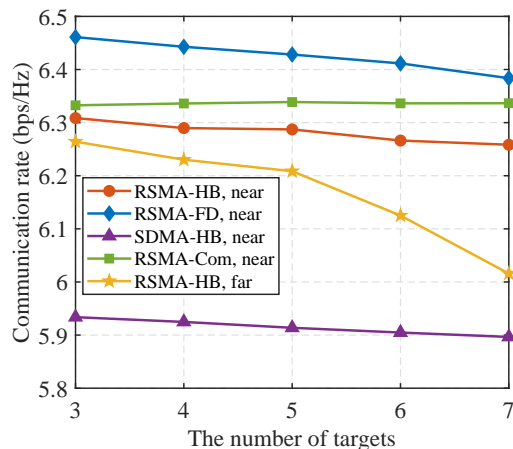


Fig. 5: Max-min communication rate versus the number of targets.

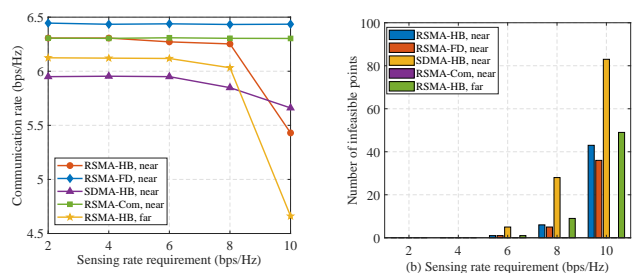


Fig. 6: (a) Max-min communication rate versus sensing rate. (b) The number of infeasible points versus the sensing rate.

increases, except for the communication-only scheme, where the communication rate remains static. This is because its performance is independent of the target numbers. Interestingly, the FF-ISAC exhibits a significant performance decline beyond five targets, rendering a more pronounced performance gap. For example, the performance gap between NF- and FF-ISACs reaches about 0.25 bps/Hz when $M = 7$. This is because targets with the same angle and distance are more likely to appear as the number of targets increases. Compared to plane-wave propagation, spherical-wave propagation encompasses distance and angle information, which can better cope with such scenarios. In addition, our proposed RSMA-based scheme consistently achieves significant performance enhancements over SDMA, about 0.35 bps/Hz. These gains again highlight the effectiveness of the proposed transmit scheme.

Fig. 6(a) illustrates the max-min communication rate versus sensing rate requirements. At the same time, Fig. 6(b) shows the number of infeasible points, reflecting instances where the sensing rate requirement is unmet across 100 channel realizations. The communication rate of all transmit schemes decreases slightly or remains static for $R_{th} < 8$ bps/Hz, indicating that multi-target detection requirements are easily supported.

Two key observations emerge for $R_{th} = 10$ bps/Hz:

- Our scheme outperforms SDMA for $R_{th} < 8$ bps/Hz but shows the opposite trend at $R_{th} = 10$ bps/Hz. This

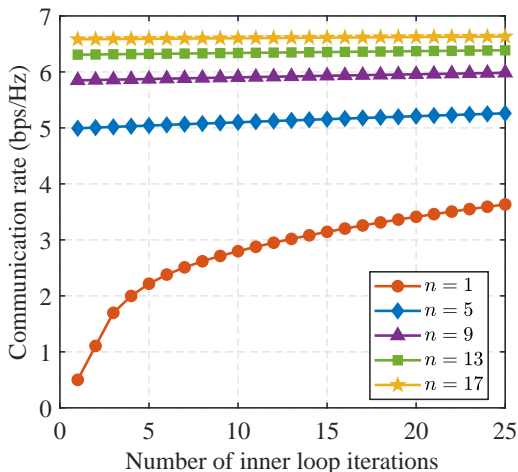


Fig. 7: Max-min communication rate versus the number of iterations, where n denotes the number of outer loop iterations.

occurs because Fig. 6(b) indicates that SDMA fails to meet the sensing rate requirement in 83% of cases at $R_{\text{th}} = 10$ bps/Hz. This lower feasible probability may overstate its performance since infeasible points, often caused by complex channel states, are discarded.

- Our transmit scheme achieves a lower infeasible probability than FF-ISAC, with a performance gain of 0.8 bps/Hz, highlighting the advantages of NF-ISAC.

Fig. 7 illustrates the convergence of the proposed PDD-based double-loop algorithm. A steady value is reached after around 17 outer loop iterations, validating the convergence analysis in Section IV. The inner loop for solving the AL problem (18) reaches a stationary value within a few iterations when the number of outer loop iterations exceeds five.

VI. CONCLUSION

This paper proposes an RSMA-based transmit scheme for NF-ISAC networks, incorporating a variable number of dedicated sensing beams. The receive filters, analog beamformer, digital communication/sensing beamformers, common rate allocation, and the number of dedicated sensing beams are jointly optimized to maximize the minimum communication rate. However, the uncertain sensing beam count and coupled beamformers make the formulated problem discrete and non-convex.

To address the high complexity of this problem, a divide-and-conquer approach is proposed. First, a solution reconstruction method is designed to determine the number of dedicated sensing beams, ensuring a globally optimal solution and a rank-zero sensing beamformer. The rank-zero structure indicates that no dedicated sensing beams are required for NF multi-target detection. Second, a PDD-based double-loop algorithm is developed to jointly optimize the remaining variables. Using WMMSE and quadratic transform techniques, communication and sensing rates are reformulated, enabling closed-form solutions for the analog beamformer, digital beamformer, and receive filters, while the auxiliary variable is efficiently solved via convex optimization.

Simulation results show that the proposed scheme performs comparably to the fully digital beamformer and communication-only networks while achieving significant gains over other benchmarks.

Our contributions provide valuable insights for future research, highlighting two key directions. First, the challenge of accurate channel estimation in NF-ISAC, which is more complex than in FF-ISAC, presents an opportunity to leverage RSMA's robustness to mitigate imperfect CSI. Second, the added complexity of mixed FF- and NF-ISAC environments suggests a promising avenue for addressing such scenarios.

APPENDIX A

PROOF OF PROPOSITION 1

The latest constructed digital beamformers yield

$$\hat{\mathbf{R}} = \sum_{k=0}^K \hat{\mathbf{W}}_k = \sum_{k=0}^K \tilde{\mathbf{W}}_k^* + \tilde{\mathbf{V}}^*, \quad (40)$$

which ensures the covariance matrix of the transmit signal remains static, yielding the same sensing rate as $\{\tilde{\mathbf{W}}_k^*, \tilde{\mathbf{V}}^*\}$. Additionally, one has

$$\begin{aligned} \sum_{k=0}^K \text{Tr} \left((\mathbf{F}^*)^H \mathbf{F}^* \hat{\mathbf{W}}_k \right) &= \sum_{k=0}^K \text{Tr} \left((\mathbf{F}^*)^H \mathbf{F}^* \left(\tilde{\mathbf{W}}_k^* + \delta_k \tilde{\mathbf{V}}^* \right) \right) \\ &\stackrel{(a)}{=} \sum_{k=0}^K \text{Tr} \left((\mathbf{F}^*)^H \mathbf{F}^* \tilde{\mathbf{W}}_k^* \right) + \text{Tr} \left((\mathbf{F}^*)^H \mathbf{F}^* \tilde{\mathbf{V}}^* \right), \end{aligned} \quad (41)$$

where equation (a) holds since $\sum_{k=0}^K \delta_k = 1$. As such, the constructed solution meets the transmit power constraint (12b) since $\{\mathbf{F}^*, \tilde{\mathbf{W}}_k^*, \tilde{\mathbf{V}}^*\}$ is a feasible point to problem (12). Then, plugging the constructed solution $\{\hat{\mathbf{W}}_k, \hat{\mathbf{V}}\}$ into $\gamma_{c,k}$, one can derive

$$\begin{aligned} \hat{\gamma}_{c,k} &= \frac{\text{Tr} \left(\mathbf{H}_k \left(\tilde{\mathbf{W}}_0^* + \delta_0 \tilde{\mathbf{V}}^* \right) \right)}{\sum_{j=1}^K \text{Tr} \left(\mathbf{H}_k \left(\tilde{\mathbf{W}}_j^* + \delta_j \tilde{\mathbf{V}}^* \right) \right) + \sigma^2} \\ &\geq \frac{\text{Tr} \left(\mathbf{H}_k \tilde{\mathbf{W}}_0^* \right)}{\sum_{j=1}^K \text{Tr} \left(\mathbf{H}_k \left(\tilde{\mathbf{W}}_j^* + \delta_j \tilde{\mathbf{V}}^* \right) \right) + \sigma^2} \\ &\geq \frac{\text{Tr} \left(\mathbf{H}_k \tilde{\mathbf{W}}_0^* \right)}{\sum_{j=1}^K \text{Tr} \left(\mathbf{H}_k \left(\tilde{\mathbf{W}}_j^* + \tilde{\mathbf{V}}^* \right) \right) + \sigma^2} = \gamma_{c,k} \end{aligned} \quad (42)$$

where the equal sign holds when $\delta_0 = 0$ and $\hat{\gamma}_{c,k}$ denotes the updated SINR. Similarly, it can be proven $\hat{\gamma}_{p,k} \geq \gamma_{p,k}$, where $\delta_0 = 0$ and $\delta_k = 0$ contributes to the equal sign. It thus can be deduced there is at least one k making $\hat{\gamma}_{p,k} > \gamma_{p,k}$ since $\sum_{k=0}^K \delta_k = 1$. This indicates that the constructed solution helps elevate the communication rate, so the objective value cannot be decreased and \mathcal{Q}_2 can satisfy constraints (11d) and (11e). Moreover, it is easy to validate that the constructed solution meets constraints (11f), (11g), (11h), and (12c). Consequently, \mathcal{Q}_2 is feasible to the problem (12) with relaxed rank-one constraint. Combining equation (40), (41), and (42), we deduce that the constructed solution can reach the same objective value as the optimal solution at least.

APPENDIX B
PROOF OF PROPOSITION 2

Without loss generality, assuming $\text{rank}(\hat{\mathbf{W}}_k) = A_k > 1$, one can derive $\hat{\mathbf{W}}_k = \sum_{i=1}^{A_k} \hat{\mathbf{w}}_{k,i} \hat{\mathbf{w}}_{k,i}^H = \hat{\mathbf{P}}_k \hat{\mathbf{P}}_k^H$ with $\hat{\mathbf{P}}_k = [\hat{\mathbf{w}}_{k,1}, \dots, \hat{\mathbf{w}}_{k,A_k}] \in \mathbb{C}^{N_f \times A_k}$. Define a Hermitian matrix $\hat{\mathbf{X}}_k \in \mathbb{C}^{A_k \times A_k}$, which lies in the left null space of $\mathbf{B}_k = [\hat{\mathbf{P}}_k^H \hat{\mathbf{B}}_1 \hat{\mathbf{P}}_k, \dots, \hat{\mathbf{P}}_k^H \hat{\mathbf{B}}_{M^2+K} \hat{\mathbf{P}}_k] \in \mathbb{C}^{A_k \times (M^2+K)A_k}$, i.e., $\text{Tr}(\mathbf{B}_k \hat{\mathbf{X}}_k) = 0$, where

$$\hat{\mathbf{B}}_i = \begin{cases} \mathbf{G}_a^H \mathbf{u}_b \mathbf{u}_b^H \mathbf{G}_a, & \text{if } i \leq M^2; \\ \mathbf{H}_{i-M^2}, & \text{if } i > M^2, \end{cases} \quad (43)$$

where $a = \lfloor i/M \rfloor$ and $b = i - aM$. Two observations can be made from the structure of \mathbf{B}_k . First, $\text{rank}(\mathbf{B}_k) \leq A_k$, which indicates that there are only A_k columns in \mathbf{B}_k are linearly independent. Second, each sub-matrix block $\hat{\mathbf{P}}_k^H \hat{\mathbf{B}}_i \hat{\mathbf{P}}_k$ is a A_k -dimension rank-one matrix since \mathbf{u}_b and \mathbf{H}_{i-M^2} are both rank-one. This reveals that linear independence cannot occur inside each sub-matrix block. Therefore, only A_k sub-matrix blocks denoted by $\{\hat{\mathbf{P}}_k^H \hat{\mathbf{B}}_j \hat{\mathbf{P}}_k\}$ with $j \in \mathcal{J} = \{1, \dots, A_k\}$ are linearly independent. The remaining $M^2 + K - A_k$ sub-matrix blocks are linearly dependent, which can be expressed by the linear combination of $\{\hat{\mathbf{P}}_k^H \hat{\mathbf{B}}_j \hat{\mathbf{P}}_k\}$ for $\forall j$. On this basis, $\text{Tr}(\mathbf{B}_k \hat{\mathbf{X}}_k) = 0$ can be reformulated as $\text{Tr}(\hat{\mathbf{P}}_k^H \hat{\mathbf{B}}_j \hat{\mathbf{P}}_k \hat{\mathbf{X}}_k) = 0$ for $\forall j$. Furthermore, since the residual sub-matrix blocks are dependent, it follows that

$$\text{Tr}(\hat{\mathbf{P}}_k^H \hat{\mathbf{B}}_i \hat{\mathbf{P}}_k \hat{\mathbf{X}}_k) = 0, \quad 1 \leq i \leq M^2 + K. \quad (44)$$

After that, a semi-definite matrix $\bar{\mathbf{W}}_k$ can be constructed as follows:

$$\bar{\mathbf{W}}_k = \hat{\mathbf{P}}_k \left(\mathbf{I} - \frac{1}{\delta_k} \mathbf{X}_k \right) \hat{\mathbf{P}}_k^H, \quad (45)$$

where δ_k is the maximal eigenvalue of \mathbf{X}_k and $\text{rank}(\bar{\mathbf{W}}_k) \leq A_k - 1$. $\bar{\mathbf{W}}_k$ is semi-definite due to $\mathbf{I} - \frac{1}{\delta_k} \mathbf{X}_k \succeq \mathbf{0}$. Combining equations (44) and (45), one finds

$$\begin{aligned} \text{Tr}(\hat{\mathbf{B}}_i \bar{\mathbf{W}}_k) &= \text{Tr}(\hat{\mathbf{B}}_i \hat{\mathbf{P}}_k \hat{\mathbf{P}}_k^H) - \frac{1}{\delta_k} \text{Tr}(\hat{\mathbf{P}}_k^H \hat{\mathbf{B}}_i \hat{\mathbf{P}}_k^H \mathbf{X}_k) \\ &\stackrel{(a)}{=} \text{Tr}(\hat{\mathbf{B}}_i \hat{\mathbf{W}}_k). \end{aligned} \quad (46)$$

This manifests that the rank-reduced matrix $\bar{\mathbf{W}}_k$ can meet constraints (12b), (12c), and (12e) in problem (12). Meanwhile, the communication rate remains unchanged, so $\bar{\mathbf{W}}_k$ can achieve the same communication performance with $\hat{\mathbf{W}}_k$ but with a lower rank. Repeating the above procedure, the rank-one solution can be obtained.

REFERENCES

- [1] Z. Ren, Y. Peng, X. Song, Y. Fang, L. Qiu, L. Liu, D. W. K. Ng, and J. Xu, "Fundamental CRB-rate tradeoff in multi-antenna ISAC systems with information multicasting and multi-target sensing," *IEEE Trans. Wireless Commun.*, vol. 23, no. 4, pp. 3870–3885, Apr. 2024.
- [2] Y. Chen, H. Hua, J. Xu, and D. W. K. Ng, "ISAC meets SWIPT: Multi-functional wireless systems integrating sensing, communication, and powering," *IEEE Trans. Wireless Commun.*, vol. 23, no. 8, pp. 8264–8280, Aug. 2024.
- [3] J. Cong, C. You, J. Li, L. Chen, B. Zheng, Y. Liu, W. Wu, Y. Gong, S. Jin, and R. Zhang, "Near-field integrated sensing and communication: Opportunities and challenges," *IEEE Wirel. Commun.*, pp. 1–8, 2024, doi=10.1109/MWC.002.2400033.
- [4] Y. Liu, Z. Wang, J. Xu, C. Ouyang, X. Mu, and R. Schober, "Near-field communications: A tutorial review," *IEEE open j. Commun. Soc.*, vol. 4, pp. 1999–2049, Aug. 2023.
- [5] Z. Zhang, Y. Liu, Z. Wang, X. Mu, and J. Chen, "Simultaneous wireless information and power transfer in near-field communications," *IEEE Internet Things J.*, vol. 11, no. 16, pp. 27760–27774, Aug. 2024.
- [6] G. Cheng, Y. Fang, J. Xu, and D. W. K. Ng, "Optimal coordinated transmit beamforming for networked integrated sensing and communications," *IEEE Trans. Wireless Commun.*, vol. 23, no. 8, pp. 8200–8214, Aug. 2024.
- [7] J. Choi, J. Park, N. Lee, and A. Alkhatieb, "Joint and robust beamforming framework for integrated sensing and communication systems," *IEEE Trans. Wireless Commun.*, pp. 1–1, 2024, doi=10.1109/TWC.2024.3454987.
- [8] Z. Liu, W. Chen, Q. Wu, J. Yuan, S. Zhang, Z. Li, and J. Li, "Rate-splitting multiple access for transmissive reconfigurable intelligent surface transceiver empowered ISAC systems," *IEEE Internet Things J.*, vol. 11, no. 16, pp. 27245–27259, Aug. 2024.
- [9] Y. Mao, B. Clerckx, and V. O. Li, "Rate-splitting multiple access for downlink communication systems: Bridging, generalizing, and outperforming SDMA and NOMA," *EURASIP J. Wireless Commun. Netw.*, vol. 2018, no. 1, pp. 1–54, May 2018.
- [10] Z. Wang, X. Mu, Y. Liu, and R. Schober, "TTD configurations for near-field beamforming: Parallel, serial, or hybrid?" *IEEE Trans. Commun.*, vol. 72, no. 6, pp. 3783–3799, Jun. 2024.
- [11] J. Zhou, C. Zhou, Y. Mao, and C. Tellambura, "Joint beam scheduling and resource allocation for flexible RSMA-aided near-field communications," *IEEE Wireless Commun. Lett.*, pp. 1–1, 2024, doi=10.1109/LWC.2024.3517151.
- [12] B. Clerckx, Y. Mao, E. A. Jorswieck, J. Yuan, D. J. Love, E. Erkip, and D. Niyato, "A primer on rate-splitting multiple access: Tutorial, myths, and frequently asked questions," *IEEE J. Select. Areas Commun.*, vol. 41, no. 5, pp. 1265–1308, May 2023.
- [13] J. Park, B. Lee, J. Choi, H. Lee, N. Lee, S.-H. Park, K.-J. Lee, J. Choi, S. H. Chae, S.-W. Jeon, K. S. Kwak, B. Clerckx, and W. Shin, "Rate-splitting multiple access for 6G networks: Ten promising scenarios and applications," *IEEE Netw.*, vol. 38, no. 3, pp. 128–136, May 2024.
- [14] Y. Mao, O. Dizdar, B. Clerckx, R. Schober, P. Popovski, and H. V. Poor, "Rate-splitting multiple access: Fundamentals, survey, and future research trends," *IEEE Commun. Surv. Tut.*, vol. 24, no. 4, pp. 2073–2126, 4th Quart. 2022.
- [15] G. Wu, Y. Fang, J. Xu, Z. Feng, and S. Cui, "Energy-efficient MIMO integrated sensing and communications with on-off nontransmission power," *IEEE Internet Things J.*, vol. 11, no. 7, pp. 12177–12191, Apr. 2024.
- [16] S. Liu, R. Liu, Z. Lu, M. Li, and Q. Liu, "Cooperative cell-free ISAC networks: Joint BS mode selection and beamforming design," in *IEEE Wireless Commun. Netw. Conf. (WCNC)*, Spr. 2024, pp. 1–6.
- [17] Z. Zhang, W. Chen, Q. Wu, Z. Li, X. Zhu, and J. Yuan, "Intelligent omni surfaces assisted integrated multi-target sensing and multi-user MIMO communications," *IEEE Trans. Commun.*, vol. 72, no. 8, pp. 4591–4606, Aug. 2024.
- [18] Z. Liu, S. Aditya, H. Li, and B. Clerckx, "Joint transmit and receive beamforming design in full-duplex integrated sensing and communications," *IEEE J. Select. Areas Commun.*, vol. 41, no. 9, pp. 2907–2919, Sept. 2023.
- [19] J. Zhou, Y. Sun, Q. Cao, and C. Tellambura, "Total delay optimization in cache-enabled C-RANs with hierarchical rate splitting," *IEEE Trans. Veh. Technol.*, vol. 71, no. 11, pp. 11832–11846, Nov. 2022.
- [20] Z. Wang, Y. Liu, X. Mu, Z. Ding, and O. A. Dobre, "NOMA empowered integrated sensing and communication," *IEEE Commun. Lett.*, vol. 26, no. 3, pp. 677–681, Mar. 2022.
- [21] L. Sun, Z. Zhao, S. Wang, Z. Ding, and M. Peng, "On the study of non-orthogonal multiple access (NOMA)-assisted integrated sensing and communication (ISAC)," *IEEE Trans. Commun.*, pp. 1–1, 2024, doi=10.1109/TCOMM.2024.3407202.
- [22] R. Zhang, K. Xiong, Y. Lu, P. Fan, D. W. K. Ng, and K. B. Letaief, "Energy efficiency maximization in RIS-assisted SWIPT networks with RSMA: A PPO-based approach," *IEEE J. Select. Areas Commun.*, vol. 41, no. 5, pp. 1413–1430, May 2023.
- [23] Y. Xu, Y. Mao, O. Dizdar, and B. Clerckx, "Max-min fairness of rate-splitting multiple access with finite blocklength communications," *IEEE Trans. Veh. Technol.*, vol. 72, no. 5, pp. 6816–6821, May 2023.
- [24] T. Zhang, Y. Zhuang, G. Chen, S. Wang, B. Lv, R. Wang, and P. Xiao, "Rate-splitting with hybrid messages: DoF analysis of the two-user MIMO broadcast channel with imperfect CSIT," *IEEE Trans. Wireless Commun.*, vol. 23, no. 9, pp. 10514–10529, Sept. 2024.

- [25] C. Meng, K. Xiong, W. Chen, B. Gao, P. Fan, and K. B. Letaief, "Sum-rate maximization in STAR-RIS-assisted RSMA networks: A PPO-based algorithm," *IEEE Internet Things J.*, vol. 11, no. 4, pp. 5667–5680, Feb. 2024.
- [26] C. Xu, B. Clerckx, S. Chen, Y. Mao, and J. Zhang, "Rate-splitting multiple access for multi-antenna joint radar and communications," *IEEE J. Sel. Top. Signal Process.*, vol. 15, no. 6, pp. 1332–1347, Nov. 2021.
- [27] K. Chen, Y. Mao, L. Yin, C. Xu, and Y. Huang, "Rate-splitting multiple access for simultaneous multi-user communication and multi-target sensing," *IEEE Trans. Veh. Technol.*, vol. 73, no. 9, pp. 13 909–13 914, Sept. 2024.
- [28] P. Gao, L. Lian, and J. Yu, "Cooperative ISAC with direct localization and rate-splitting multiple access communication: A pareto optimization framework," *IEEE J. Select. Areas Commun.*, vol. 41, no. 5, pp. 1496–1515, May 2023.
- [29] Z. Chen, J. Wang, Z. Tian, M. Wang, Y. Jia, and T. Q. S. Quek, "Joint rate splitting and beamforming design for RSMA-RIS-assisted ISAC system," *IEEE Wireless Commun. Lett.*, vol. 13, no. 1, pp. 173–177, Jan. 2024.
- [30] Z. Liu, L. Yin, W. Shin, and B. Clerckx, "Rate-splitting multiple access for quantized ISAC LEO satellite systems: A max-min fair energy-efficient beam design," *IEEE Trans. Wireless Commun.*, vol. 23, no. 10, pp. 15 394–15 408, Oct. 2024.
- [31] A. Hakimi, D. Galappaththige, and C. Tellambura, "A roadmap for NF-ISAC in 6G: A comprehensive overview and tutorial," *Entropy*, vol. 26, no. 9, p. 773, Sept. 2024.
- [32] D. Galappaththige, S. Zargari, C. Tellambura, and G. Y. Li, "Near-field ISAC: Beamforming for multi-target detection," *IEEE Wireless Commun. Lett.*, vol. 13, no. 7, pp. 1938–1942, Jul. 2024.
- [33] Z. Wang, X. Mu, and Y. Liu, "Near-field integrated sensing and communications," *IEEE Commun. Lett.*, vol. 27, no. 8, pp. 2048–2052, Aug. 2023.
- [34] H. Li, Z. Wang, X. Mu, P. Zhiwen, and Y. Liu, "Near-field integrated sensing, positioning, and communication: A downlink and uplink framework," *IEEE J. Select. Areas Commun.*, vol. 42, no. 9, pp. 2196–2212, Sept. 2024.
- [35] I. Gavras and G. C. Alexandropoulos, "Simultaneous near-field THz communications and sensing with full duplex metasurface transceivers," in *IEEE 25th Int. Workshop Signal Process. Adv. Wireless Commun.*, 2024, pp. 126–130.
- [36] M. Lu, H. Luo, R. Liu, M. Li, and Q. Liu, "Beamforming design for near-field integrated sensing and communications," in *IEEE 23rd Int. Conf. Commun. Technol. (ICCT)*, Oct. 2023, pp. 434–438.
- [37] G. Zheng, M. Wen, J. Wen, and C. Shan, "Joint hybrid precoding and rate allocation for RSMA in near-field and far-field massive MIMO communications," *IEEE Wireless Commun. Lett.*, vol. 13, no. 4, pp. 1034–1038, Apr. 2024.
- [38] J. An, C. Yuen, L. Dai, M. Di Renzo, M. Debbah, and L. Hanzo, "Near-field communications: Research advances, potential, and challenges," *IEEE Wirel. Commun.*, vol. 31, no. 3, pp. 100–107, Jun. 2024.
- [39] E. Bjrnson, C. B. Chae, R. W. Heath, T. L. Marzetta, A. Mezghani, L. Sanguinetti, F. Rusek, M. R. Castellanos, D. Jun, and Z. T. Demir, "Towards 6G MIMO: Massive spatial multiplexing, dense arrays, and interplay between electromagnetics and processing," *arXiv preprint arXiv:2401.02844*, 2024.
- [40] S. Lv, Y. Liu, X. Xu, A. Nallanathan, and A. L. Swindlehurst, "RIS-aided near-field MIMO communications: Codebook and beam training design," *IEEE Trans. Wireless Commun.*, vol. 23, no. 9, pp. 12 531–12 546, Sept. 2024.
- [41] Q. Shi and M. Hong, "Penalty dual decomposition method for non-smooth nonconvex optimization—part I: Algorithms and convergence analysis," *IEEE Trans. Signal Process.*, vol. 68, pp. 4108–4122, Jun. 2020.
- [42] J. Zhang, B. Clerckx, J. Ge, and Y. Mao, "Cooperative rate splitting for MISO broadcast channel with user relaying, and performance benefits over cooperative NOMA," *IEEE Signal Process. Lett.*, vol. 26, no. 11, pp. 1678–1682, Nov. 2019.
- [43] K. Shen and W. Yu, "Fractional programming for communication systems—part I: Power control and beamforming," *IEEE Trans. Signal Process.*, vol. 66, no. 10, pp. 2616–2630, May 2018.
- [44] Z. Zhang, Y. Liu, Z. Wang, X. Mu, and J. Chen, "Physical layer security in near-field communications," *IEEE Trans. Veh. Technol.*, vol. 73, no. 7, pp. 10 761–10 766, Jul. 2024.